Article - Control

TRANSACTIONS OF THE INSTITUTE OF MEASUREMENT & CONTROL

Transactions of the Institute of Measurement and Control
2021, Vol. 43(5) 1143–1155

DOI: 10.1177/0142331220966427
journals.sagepub.com/home/tim
SAGE

Extended state observer-based robust control of an omnidirectional quadrotor with tiltable rotors

Kaiwen Lu[1], Zhong Yang[1], Luwei Liao[1], Yuhong Jiang[2], Changliang Xu[1], Hao Xu[1] and Qiuyan Zhang[3]

Abstract

A quadrotor with tiltable rotors is a kind of omnidirectional multirotor aerial vehicle (MAV) that has demonstrated advantages of decoupling control of position from the control of orientation. However, quadrotors with tiltable rotors usually suffer from Coriolis term, modeling error and external disturbance. To this end, the extended state observer (ESO)-based controller is designed to estimate and compensate for the above adverse effects. Especially, the controller involves position and attitude controller in parallel. The attitude controller is made up of cascade control-loops: an outer quaternion-based attitude control-loop and an inner ESO-based Proportional derivative angular velocity control-loop. Similarly, the position controller consists of an outer proportional position control-loop and an inner ESO-based PD velocity control-loop. Besides, a linear control allocation strategy, which allocates the controller outputs to tilting angles and motor speed directly, is proposed to avoid the nonlinear allocation matrix. Extensive simulations and flight tests are carried out to illustrate the effectiveness and robustness of the proposed ESO-based controller.

Keywords

Omnidirectional MAV, extended state observer, disturbance rejection, PD control, control allocation

Introduction

In the research community, there is an increasing interest to transition the use of multirotor aerial vehicles (MAVs) from passive tasks, such as aerial photography, surveying, and traffic monitoring, to active interaction tasks for instance, load transportation (Gassner et al., 2017), valve turning (Korpela et al. (2014)) and aerial grasping (Thomas et al., 2014). Among the various challenges faced by traditional MAVs, such as limited payload capacity, unsatisfying duration of flight, uncertainties in outdoor environment, an important one is the underactuation (Rajappa et al., 2015), that is, the inability to exert the 6 degrees of freedom (DoF) force and torque. In most researches and applications, quadrotors have been used as the main platform. However, they are also underactuated and can only exert force to their vertical direction in the body frame. This is reason why quadrotors need to roll and pitch to achieve accelerations in the horizontal direction.

Several novel fully-actuated MAVs have been designed as solutions to the underactuated problem with conventional MAVs (Crowther et al., 2011; Rashad et al., 2019; Ryll et al., 2015, 2016). Due to the ability to generate forces and torques in all directions, fully-actuated MAVs has omnidirectional flight capabilities and improved maneuverability. Regarding omnidirectional MAVs, there are two common approaches in the literature. The first approach is to endow multirotor systems with non-coplanar tilted rotors. The omnicopter presented by Dyer et al. (2019) used intelligent rotor configuration in a cube-like structure to produce all the six DoFs forces and torques. Park et al. (2016) and Park et al. (2018) proposed a novel multi-rotor flying platform, featuring six opportunistically distributed rotors, to attain omnidirectional motion. However, the constant presence of internal forces significantly reduces the efficiency and hence flight time (Kamel et al., 2018). The second common approach for fully-actuated MAVs is the use of tilting rotors that promises to address some of the above challenges. To the best of our knowledge, Ryll et al. (2012) and Ryll et al. (2013) first presented the concept for quadrotors involving tilting rotors and illustrated the hardware/software specifications of the developed prototype. Oosedo et al. (2015) is also involved with tilting rotors, but only considered flight modes in the horizontal orientation and the vertical orientation. The work of Kaufman et al. (2014) included the design of a nonlinear geometric controller for an omnidirectional hexarotor with tilting

[1]College of Automation Engineering, Nanjing University of Aeronautics and Astronautics, P.R. China
[2]Research Institute of UAV, Nanjing University of Aeronautics and Astronautics, P.R. China
[3]Guizhou Power Grid Company Limited, P.R. China

Corresponding author:
Zhong Yang, College of Automation Engineering, Nanjing University of Aeronautics and Astronautics, No. 29 Jiang Jun Road, Jiang Ning District, Nanjing, Jiangsu 211106, P.R. China.
Email: yangzhong@nuaa.edu.cn

rotors, but only considered the control of orientation. Kamel et al. (2018) proposed a novel control allocation strategy for jointly controlling position and orientation in the Voliro system, and experimentally evaluated the agility of the system.

While the previously discussed works were demonstrated in numeric simulations or real-world experiments, coriolis term, and external disturbance are not token into consideration in these tilting rotor system. It is widely known that the performance of multirotor is affected by the Coriolis effects (Chovancov et al., 2014; Pounds et al., 2010) and the multirotor dynamic is quite sensitive to the external disturbance (Barikbin and Fakharian, 2019; Liu et al., 2017). Most of the proposed controllers are designed based on assumptions of the knowledge of the inertia matrix (for the purpose of feedforwarding the Coriolis term) and the absence of external disturbance. In fact, the inertia matrix parameter is difficult to identify, and the external disturbance does exist in many application scenarios like windy environments. A fairly common method to deal with the above adverse effects in the aerial vehicle research community is involving observers such as disturbance observer (Castillo et al., 2019; Lazim et al., 2019), extended state observer (ESO) (He and He, 2018; Shi et al., 2019) and sliding mode observer (Benallegue et al., 2008), which can effectively estimate the disturbance and uncertainty. The ESO can estimate both the total disturbances and the states of the system with less knowledge of model information (Han, 2009; Wang and Gao, 2003). The main idea behind it is to view the unknown plant dynamics, uncertainty, and external disturbance as total disturbance, and utilize observer to estimate the total disturbance in real time as an extended state. A sliding mode controller-based ESO was designed in Liu et al. (2017). The work presented in Yao et al. (2014) employed ESO-based nonlinear control for designing a robust controller. Although the ESO is involved in many applications, there is no research on the applications of the ESO in quadrotors with tiltable rotors under the external disturbances.

Motivated by the above observations, an ESO-based robust omnidirectional control method is proposed for a quadrotor with tiltable rotors (as shown in Figure 1) subject to Coriolis effects, system uncertainties, and external disturbances. Different from the previously proposed hierarchical control structure for standard quadrotors, the position controller and attitude controller in this paper adopt a parallel structure due to the decoupling property between translational and rotational subsystems. The position controller that controls the thrust force acting on the vehicle is designed in two steps. For the first step, a cascade proportional derivative (PD) controller is firstly designed to track desired position, then a second-order linear ESO is involved in the velocity control-loop to estimate and compensate the uncertainties and disturbances. The attitude controller that controls the moments acting on the vehicle is designed almost in the same way. In particular, the outer control-loop of the attitude controller is based on quaternion algebra for aggressive attitude maneuvers. Furthermore, a linear control allocation strategy based on variable substitution is extended, so that the outputs of the designed controllers are directly mapped to the motor speed and tilting angles.

In summary, the contributions of this paper are as follows:

Figure 1. Prototype of the quadrotor with tiltable rotors.

(i) An introduction of a control structure that handles unknown variable aerodynamics efforts;
(ii) A flight control structure in parallel proposed due to the decouple property between translational and rotational subsystems;
(iii) An ESO-based linear control designed to improve robustness of the tilting rotor system;
(iv) A linear control allocation strategy proposed to avoid the nonlinear allocation matrix.

The rest of the paper is organized as follows. Section 2 briefly describes the dynamic model of the quadrotor with tiltable rotors. Section 3 introduces the ESO-based omnidirectional control and control allocation strategy. Section 4 analyzes the observer stability and cloesd-loop stability. Extensive numerical simulations are presented in Section 5, while conclusions and future directions will be explained in Section 6.

Mathematical model

Notations and preliminaries

Let $\mathcal{F}_W : \{\boldsymbol{O}_W : \boldsymbol{X}_W, \boldsymbol{Y}_W, \boldsymbol{Z}_W\}$ denote the world inertial frame fixed on the ground, and $\mathcal{F}_B : \{\boldsymbol{O}_B : \boldsymbol{X}_B, \boldsymbol{Y}_B, \boldsymbol{Z}_B\}$ denote the body frame attached to the vehicle body at the center of gravity, as seen in Figure 2. There are also four frames of the propeller groups $\mathcal{F}_{P_i} : \{\boldsymbol{O}_{P_i} : \boldsymbol{X}_{P_i}, \boldsymbol{Y}_{P_i}, \boldsymbol{Z}_{P_i}\}$ shown in Figure 3. These frames rotate around their $\boldsymbol{X}_{P_i}$ axes, w.r.t the body frame.

As usual, the rotation matrix ${}^{W}\boldsymbol{R}_B$ stands for the orientation of the vehicle body frame w.r.t world inertial frame while ${}^{B}\boldsymbol{R}_{P_i}$ stands for the orientation of the i-th propeller group frame w.r.t body frame. By denoting the propeller tilting angle around the axis $\boldsymbol{X}_{P_i}$ with α_i, it follows that

$$ {}^{B}\boldsymbol{R}_{P_i} = \boldsymbol{R}_Z\left(\frac{\pi}{2}i + \frac{\pi}{4}\right)\boldsymbol{R}_X(\alpha_i), i = 1 \ldots 4. \tag{1} $$

Also let

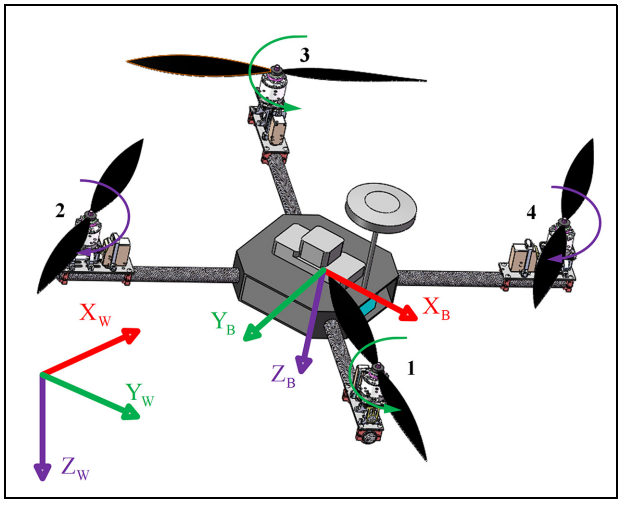

Figure 2. The world and body coordinate system.

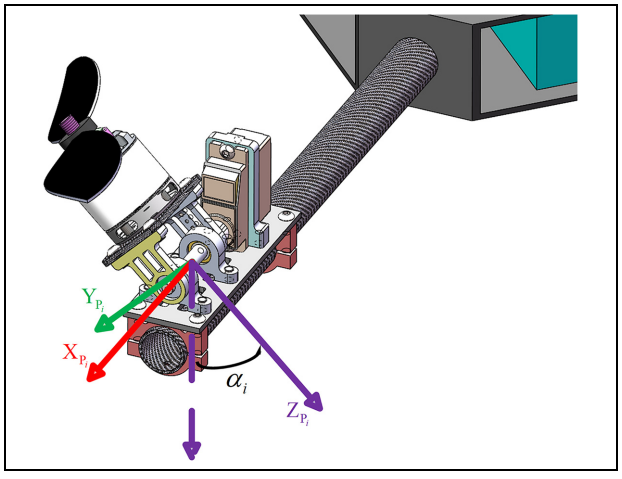

Figure 3. The propeller group coordinate system.

$$\boldsymbol{O}_{P_i}^{B} = \boldsymbol{R}_Z\left(\frac{\pi}{2}i + \frac{\pi}{4}\right)\begin{bmatrix} l \\ 0 \\ 0 \end{bmatrix}, \tag{2}$$

be the origin of $\mathcal{F}_{P_i}$ in $\mathcal{F}_B$ with l being the distance between $\boldsymbol{O}_{P_i}$ and $\boldsymbol{O}_B$.

A unit quaternion is defined as $\boldsymbol{q} = [\,q_0 \quad \boldsymbol{q}_v\,]^T$ with the real part q_0 and the vector part $\boldsymbol{q}_v$. The associated rotation matrix $\boldsymbol{R}$ is given by the Euler-Rodrigues formula (Shuster,1993)

$$\boldsymbol{R}(\boldsymbol{q}) = (q_0^2 - \boldsymbol{q}_v{}^T\boldsymbol{q}_v)\boldsymbol{I}_3 + 2\boldsymbol{q}_v\boldsymbol{q}_v{}^T + 2q_0\boldsymbol{S}(\boldsymbol{q}_v), \tag{3}$$

where $\boldsymbol{S}(\boldsymbol{q}_v)$ denotes the skew-matrix of $\boldsymbol{q}_v$

$$\boldsymbol{S}(\boldsymbol{q}_v) = \begin{bmatrix} 0 & -q_3 & q_2 \\ q_3 & 0 & -q_1 \\ -q_2 & q_1 & 0 \end{bmatrix}.$$

The combined rotation of two given rotations $\boldsymbol{q}_1$ and $\boldsymbol{q}_2$ is expressd by their multiplication $\boldsymbol{q}_1 \circ \boldsymbol{q}_2$. Also, the rotations are non-commutative, $\boldsymbol{q}_1 \circ \boldsymbol{q}_2 \neq \boldsymbol{q}_2 \circ \boldsymbol{q}_1$.

Kinematic model

Let v be the quadrotor velocity in the world frame, and $\boldsymbol{\omega}$ be the quadrotor angular velocity in the body frame. Also, $\boldsymbol{p} = \boldsymbol{O}_B^W$ is the position of the quadrotor in the world frame. The translation and quaternion-based rotation kinematic model can be described as

$$\begin{cases} \dot{\boldsymbol{p}} = \boldsymbol{v}, \\ \dot{q}_0 = -\dfrac{1}{2}\boldsymbol{q}_v{}^T\boldsymbol{\omega}, \\ \dot{\boldsymbol{q}}_v = \dfrac{1}{2}[q_0\boldsymbol{I}_3 + \boldsymbol{S}(\boldsymbol{q}_v)]\boldsymbol{\omega}^B. \end{cases} \tag{4}$$

Dynamic model

By utilizing the Newton-Euler procedure for dynamic systems, it is possible to derive the complete dynamic model of the quadrotor by considering the forces and moments generated by each propeller rotation together with the significant Coriolis effects, gyroscopic effects and external disturbances. According to Ryll et al. (2012) and Rajappa et al. (2015), it follows that: the translation dynamics described in $\mathcal{F}_W$ are

$$m\dot{\boldsymbol{v}} = m\begin{bmatrix} 0 \\ 0 \\ g \end{bmatrix} + \boldsymbol{F} + \boldsymbol{F}_\delta, \tag{5}$$

where m is the quadrotor mass, g is the scalar gravity constant, $\boldsymbol{F}_\delta$ represents the unmodeled effects and external disturbances, and $\boldsymbol{F}$ is the input forces, which is expressed in $\mathcal{F}_W$ by

$$\boldsymbol{F} = {}^W\boldsymbol{R}_B\sum_{i=1}^{4}{}^B\boldsymbol{R}_{P_i}\boldsymbol{T}_i, \tag{6}$$

where $\boldsymbol{T}_i$ is the thrust produced by the i-th propeller group. The thrust expressed in $\mathcal{F}_W$ is then

$$\boldsymbol{T}_i = \begin{bmatrix} 0 & 0 & k_f n_i^2 \end{bmatrix}^T, \tag{7}$$

where n_i is the spinning velocity of the i-th propeller and $k_f > 0$ is the thrust coefficient.

Assumption 1: The unmodeled effects and external disturbance in translation dynamics, $\boldsymbol{F}_\delta$, is continuous with bounded first derivative, that is, $\left\|\dot{\boldsymbol{F}}_\delta\right\| \leqslant \beta_{\dot{F}_\delta}$ for some $\beta_{\dot{F}_\delta} \geqslant 0$.

Then rotation dynamics described in $\mathcal{F}_B$ are

$$\boldsymbol{J}_B\dot{\boldsymbol{\omega}} = -\boldsymbol{\omega} \times \boldsymbol{J}_B\boldsymbol{\omega} + \boldsymbol{M} + \boldsymbol{M}_\delta, \tag{8}$$

where $\boldsymbol{J}_B$ is the quadrotor inertia matrix, $\boldsymbol{M}_\delta$ stands for external disturbances and unmodeled effects, and $\boldsymbol{M}$ is the input moments, which is expressed in $\mathcal{F}_B$ as

$$\boldsymbol{M} = \boldsymbol{M}_{thrust} + \boldsymbol{M}_{drag}, \tag{9}$$

where $\boldsymbol{M}_{thrust}$ is generated by the four propeller thrusts and $\boldsymbol{M}_{drag}$ is counter-rotating moment caused by air drag. The thrust moment and counter-rotating moment expressd in $\mathcal{F}_B$ are

$$\boldsymbol{M}_{thrust} = \sum_{i=1}^{4} \left(\boldsymbol{O}_{P_i}^{B} \times {}^{B}\boldsymbol{R}_{P_i} \boldsymbol{T}_i \right), \tag{10}$$

$$\boldsymbol{M}_{drag} = \sum_{i=1}^{4} {}^{B}\boldsymbol{R}_{P_i}((-1)^{i-1} c_d \boldsymbol{T}_i), \tag{11}$$

where $c_d > 0$ is the lift-to-drag ratio.

Assumption 2: The unmodeled effects and external disturbance in rotation dynamics, $\boldsymbol{M}_\delta$, is continuous with bounded first derivative, that is, $\|\dot{\boldsymbol{M}}_\delta\| \leq \beta_{\dot{M}_\delta}$ for some $\beta_{\dot{M}_\delta} \geq 0$.

Using (5)–(11), the dynamics of quadrotor with tiltable rotors are given by

$$\begin{cases} \dot{\boldsymbol{v}} = \boldsymbol{B}_v(m\boldsymbol{g} + \boldsymbol{F}) + \boldsymbol{\delta}_f(\boldsymbol{v}, \dot{\boldsymbol{v}}, t), \\ \dot{\boldsymbol{\omega}} = \boldsymbol{B}_\omega \boldsymbol{M} + \boldsymbol{\delta}_m(\boldsymbol{\omega}, \dot{\boldsymbol{\omega}}, t), \end{cases} \tag{12}$$

where

$$\begin{aligned} &\boldsymbol{B}_v = \frac{1}{m}\boldsymbol{I}_3, \boldsymbol{B}_\omega = \boldsymbol{J}_B^{-1}, \\ &\boldsymbol{\delta}_f(\boldsymbol{v}, \dot{\boldsymbol{v}}, t) = \boldsymbol{B}_v \boldsymbol{F}_\delta, \\ &\boldsymbol{\delta}_m(\boldsymbol{\omega}, \dot{\boldsymbol{\omega}}, t) = \boldsymbol{B}_{\boldsymbol{\omega}}(-\boldsymbol{\omega} \times \boldsymbol{I}_B \boldsymbol{\omega} + \boldsymbol{M}_\delta). \end{aligned}$$

Remark 1: Note that $\boldsymbol{\delta}_f(\boldsymbol{v}, \dot{\boldsymbol{v}}, t)$ and $\boldsymbol{\delta}_m(\boldsymbol{\omega}, \dot{\boldsymbol{\omega}}, t)$ contain the total force disturbances and moments disturbances, including Coriolis effects, gyroscopic effects, unmodeled effects, and the external disturbances. The ESO will estimate the two term in real time.

The relation between input forces, input moments, tilting angles, and propeller spinning velocities can then be described by

$$\begin{bmatrix} {}^{B}\boldsymbol{R}_W \boldsymbol{F} \\ \boldsymbol{M} \end{bmatrix} = \boldsymbol{A}(\alpha) \begin{bmatrix} n_1^2 \\ n_2^2 \\ n_3^2 \\ n_4^2 \end{bmatrix}, \tag{13}$$

where $\boldsymbol{A}(\alpha) \in \mathcal{R}^{6\times 4}$ referred as allocation matrix, is shown in (14) with $c(\cdot)$ representing the cosine and $s(\cdot)$ representing the sine

$$\boldsymbol{A}(\alpha) = \begin{bmatrix} -\frac{\sqrt{2}}{2}k_f s(\alpha_1) & -\frac{\sqrt{2}}{2}k_f s(\alpha_2) & \frac{\sqrt{2}}{2}k_f s(\alpha_3) & \frac{\sqrt{2}}{2}k_f s(\alpha_4) \\ \frac{\sqrt{2}}{2}k_f s(\alpha_1) & -\frac{\sqrt{2}}{2}k_f s(\alpha_2) & -\frac{\sqrt{2}}{2}k_f s(\alpha_3) & \frac{\sqrt{2}}{2}k_f s(\alpha_4) \\ -k_f c(\alpha_1) & -k_f c(\alpha_2) & -k_f c(\alpha_3) & -k_f c(\alpha_4) \\ \frac{\sqrt{2}}{2}k_f(c_d s(\alpha_1) - lc(\alpha_1)) & -\frac{\sqrt{2}}{2}k_f(lc(\alpha_2) + c_d s(\alpha_2)) & \frac{\sqrt{2}}{2}k_f(lc(\alpha_3) - c_d s(\alpha_3)) & \frac{\sqrt{2}}{2}k_f(lc(\alpha_4) + c_d s(\alpha_4)) \\ \frac{\sqrt{2}}{2}k_f(lc(\alpha_1) - c_d s(\alpha_1)) & -\frac{\sqrt{2}}{2}k_f(lc(\alpha_2) + c_d s(\alpha_2)) & \frac{\sqrt{2}}{2}k_f(c_d s(\alpha_3) - lc(\alpha_3)) & \frac{\sqrt{2}}{2}k_f(lc(\alpha_4) + c_d s(\alpha_4)) \\ k_f(ls(\alpha_1) + c_d c(\alpha_1)) & k_f(ls(\alpha_2) - c_d c(\alpha_2)) & k_f(ls(\alpha_3) + c_d c(\alpha_3)) & k_f(ls(\alpha_4) - c_d c(\alpha_4)) \end{bmatrix}. \tag{14}$$

Control design

Control structure

In this section, a flight controller is presented for the omnidirectional quadrotor with tiltable rotors. Due to the independent actual forces and moments, the position and rotation dynamics are decoupled. Therefore, a control structure (Figure 4) where position and attitude controllers are in parallel is considered to control the quadrotor position and orientation jointly.

Moreover, the ESO technique is applied to estimate the unmodeled effects and external disturbances in equations (5)

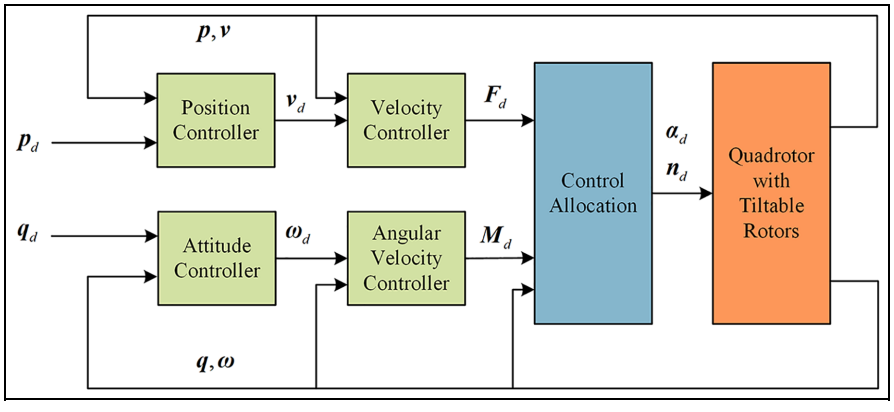

Figure 4. The proposed control structure.

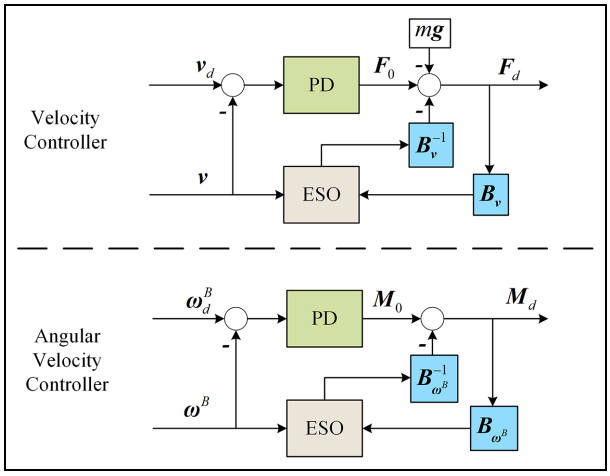

Figure 5. The proposed ESO-based inner control-loop.

and (8). As shown in Figure 5, the ESO operates in the inner control-loop.

Position control

The position control is formed by two cascade controllers: an outer position control-loop generating the desired velocity $\boldsymbol{v}_d$ and an inner velocity control-loop generating the desired force vector F_d. Let $\boldsymbol{p}_d$ be the desired position, and then the position error $\boldsymbol{p}_e = \boldsymbol{p}_d - \boldsymbol{p}$ be defined as the difference between the desired position and current position. Generally, the desired velocity is given by

$$\boldsymbol{v}_d = \boldsymbol{K}\boldsymbol{p}_e, \tag{15}$$

where the $\boldsymbol{K} = \mathrm{diag}[k_x \quad k_y \quad k_z]$ are the position controller gains.

Then, the desired forces $\boldsymbol{F}_d$ are computed as

$$\boldsymbol{F}_0 = \boldsymbol{K}_{v,p}\boldsymbol{v}_e + \boldsymbol{K}_{v,d}\dot{\boldsymbol{v}}_e, \tag{16}$$

$$\boldsymbol{F}_d = \boldsymbol{B}_v^{-1}\boldsymbol{F}_0 - m\boldsymbol{g} + \boldsymbol{F}_{oc}, \tag{17}$$

where $\boldsymbol{K}_{v,p} = \mathrm{diag}\left[k_{v_x,p} \quad k_{v_y,p} \quad k_{v_z,p}\right]$ and $\boldsymbol{K}_{v,d} = \mathrm{diag}\left[k_{v_x,d} \quad k_{v_y,d} \quad k_{v_z,d}\right]$ are the velocity controller gains and $\boldsymbol{F}_{oc}$ is the compensation term of $\delta_f(v, \dot{v}, t)$, which is given by the following ESO.

Define $\boldsymbol{\xi} = [\boldsymbol{\xi}_1 \quad \boldsymbol{\xi}_2]^T = [\boldsymbol{v} \quad \boldsymbol{\delta}_f(\boldsymbol{v}, \dot{\boldsymbol{v}}, t)]^T$. In order to construct the observer, the uncertain system in translation dynamics is augmented as

$$\begin{cases} \dot{\boldsymbol{\xi}}_1 = \boldsymbol{B}_v(m\boldsymbol{g} + \boldsymbol{F}) + \boldsymbol{\xi}_2, \\ \dot{\boldsymbol{\xi}}_2 = \boldsymbol{h}(\boldsymbol{\xi}), \\ \boldsymbol{y} = \boldsymbol{\xi}_1. \end{cases} \tag{18}$$

Here, $\boldsymbol{h}(\boldsymbol{\xi}) = \dot{\boldsymbol{\delta}}_f(\boldsymbol{v}, \dot{\boldsymbol{v}}, t)$ is assumed to be a unknown but bounded function. With $\boldsymbol{F}$ and $\boldsymbol{y}$ being inputs and $\hat{\boldsymbol{\xi}} = \left[\hat{\boldsymbol{\xi}}_1 \quad \hat{\boldsymbol{\xi}}_2\right]^T$ being the estimation of $\boldsymbol{\xi}$, the ESO of (17) is given as

$$\begin{cases} \dot{\hat{\boldsymbol{\xi}}}_1 = \boldsymbol{B}_v(m\boldsymbol{g} + \boldsymbol{F}) + \hat{\boldsymbol{\xi}}_2 + \boldsymbol{\beta}_{\xi,1}(\boldsymbol{\xi}_1 - \hat{\boldsymbol{\xi}}_1), \\ \dot{\hat{\boldsymbol{\xi}}}_2 = \boldsymbol{\beta}_{\xi,2}(\boldsymbol{\xi}_1 - \hat{\boldsymbol{\xi}}_1), \end{cases} \tag{19}$$

where $\boldsymbol{\beta}_{\xi,1} = \beta_{\xi,1}\boldsymbol{I}$ and $\boldsymbol{\beta}_{\xi,2} = \beta_{\xi,2}\boldsymbol{I}$ are the observer gains to be chosen. With a well-tuned ESO, the compensation term of $\boldsymbol{\delta}_f(\boldsymbol{v}, \dot{\boldsymbol{v}})$ can be calculated as

$$\boldsymbol{F}_{oc} = -\boldsymbol{B}_v^{-1}\hat{\boldsymbol{\xi}}_2. \tag{20}$$

Therefore, the original translation dynamics should be approximately reduced to

$$\dot{\boldsymbol{v}} \approx \boldsymbol{F}_0, \tag{21}$$

which can be easily controlled by the control law (16).

Attitude control

The attitude control also consists of an outer attitude control-loop generating the desired angular velocity $\boldsymbol{\omega}_d$ and an inner angular velocity control-loop generating the desired moments $\boldsymbol{M}_d$. In order to carry out aggressive attitude maneuvers, the attitude control-loop is based on quaternion. The attitude error, q_e, is defined as the difference between the desired attitude $\boldsymbol{q}_d$ and the current attitude $\boldsymbol{q}$, and it can be computed by

$$\boldsymbol{q}_e = \boldsymbol{q}^{-1} \circ \boldsymbol{q}_d = \begin{bmatrix} q_{0,e} \\ \boldsymbol{q}_{v,e} \end{bmatrix} \tag{22}$$

Then the desired angular velocity $\boldsymbol{\omega}_d$ is given from the vector part $\boldsymbol{q}_{v,e}$ of the quaternion error by

$$\boldsymbol{\omega}_d = -k_q \mathrm{sign}(q_{0,e})\boldsymbol{q}_{v,e} \tag{23}$$

where k_q is the attitude position controller gain.

Remark 2: It is guaranteed that the rotation angle is always no more than π by taking the sign of $q_{e,0}$. This means that the attitude controller always rotates the quadrotor from current attitude $\boldsymbol{q}$ to the desired $\boldsymbol{q}_d$ in such a way that the rotation angle is minimal.

Remark 3: As $\|\boldsymbol{q}\| = 1$ by definition, $\|\boldsymbol{q}_{v,e}\| \leqslant 1$. Therefore, the generated maximal possible desired angular velocity is limited to $\|\boldsymbol{\omega}_d\| \leqslant k_q$. This is an advantage due to the real quadrotor rotation speed has saturation.

The proposed angular velocity control law is

$$\boldsymbol{M}_0 = \boldsymbol{K}_{\omega,p}\boldsymbol{\omega}_e + \boldsymbol{K}_{\omega,d}\dot{\boldsymbol{\omega}}_e, \tag{24}$$

$$\boldsymbol{M}_d = \boldsymbol{B}_\omega^{-1}\boldsymbol{M}_0 + \boldsymbol{M}_{oc}, \tag{25}$$

where $\boldsymbol{K}_{\omega,p} = \mathrm{diag}\left[k_{\omega_x,p} \quad k_{\omega_y,p} \quad k_{\omega_z,p}\right]$ and $\boldsymbol{K}_{\omega,d} = \mathrm{diag}\left[k_{\omega_x,d} \quad k_{\omega_y,d} \quad k_{\omega_z,d}\right]$ are the angular velocity controller gains and $\boldsymbol{M}_{oc}$ is the compensation term of $\boldsymbol{\delta}_m(\boldsymbol{\omega}, \dot{\boldsymbol{\omega}}, t)$, which is given by the following ESO.

Define $\boldsymbol{\zeta} = [\boldsymbol{\zeta}_1 \quad \boldsymbol{\zeta}_2]^T = [\boldsymbol{\omega} \quad \boldsymbol{\delta}_m(\boldsymbol{\omega}, \dot{\boldsymbol{\omega}}, t)]^T$. To construct the observer, the uncertain system in rotation dynamics is augmented as

$$\begin{cases} \dot{\boldsymbol{\zeta}}_1 = \boldsymbol{B}_\omega \boldsymbol{M} + \boldsymbol{\zeta}_2, \\ \dot{\boldsymbol{\zeta}}_2 = \boldsymbol{h}(\boldsymbol{\zeta}), \\ \boldsymbol{y} = \boldsymbol{\zeta}_1. \end{cases} \tag{26}$$

Here, $\boldsymbol{h}(\boldsymbol{\zeta}) = \dot{\boldsymbol{\delta}}_m(\boldsymbol{\omega}, \dot{\boldsymbol{\omega}}, t)$ is assumed to be an unknown but bounded function. With $\boldsymbol{M}$ and $\boldsymbol{y}$ being inputs and $\hat{\boldsymbol{\zeta}} = \begin{bmatrix} \hat{\boldsymbol{\zeta}}_1 & \hat{\boldsymbol{\zeta}}_2 \end{bmatrix}^T$ being the estimation of $\boldsymbol{\zeta}$, the ESO of (25) is given as

$$\begin{cases} \dot{\hat{\boldsymbol{\zeta}}}_1 = \boldsymbol{B}_\omega \boldsymbol{M} + \hat{\boldsymbol{\zeta}}_2 + \boldsymbol{\beta}_{\zeta,1}(\boldsymbol{\zeta}_1 - \hat{\boldsymbol{\zeta}}_1), \\ \dot{\hat{\boldsymbol{\zeta}}}_2 = \boldsymbol{\beta}_{\zeta,2}(\boldsymbol{\zeta}_1 - \hat{\boldsymbol{\zeta}}_1), \end{cases} \tag{27}$$

where $\boldsymbol{\beta}_{\zeta,1} = \beta_{\zeta,1}\boldsymbol{I}$ and $\boldsymbol{\beta}_{\zeta,2} = \beta_{\zeta,2}\boldsymbol{I}$ are the observer gains to be chosen. With a well-tuned ESO, the compensation term of $\boldsymbol{\delta}_m(\boldsymbol{\omega}, \dot{\boldsymbol{\omega}}, t)$ can be calculated as

$$\boldsymbol{M}_{oc} = -\boldsymbol{B}_\omega^{-1}\hat{\boldsymbol{\zeta}}_2. \tag{28}$$

Therefore, the original rotation dynamics should be approximately reduced to

$$\dot{\boldsymbol{\omega}} \approx \boldsymbol{M}_0, \tag{29}$$

which can be easily controlled by the control law (24).

Control allocation

The last step of the controller is to allocate the forces and moments to rotors. The allocation matrix in (13) is a function of tilting angles α while it is a constant matrix for standard quadrotors. Through the selection of appropriate tilting angles, the force vector can be directed not only in the $\boldsymbol{Z}_B$ direction but also in the $\boldsymbol{X}_B$ and $\boldsymbol{Y}_B$ direction. However, the tilting angles appear as a nonlinear term in the allocation matrix. Besides, the control allocation solution is not unique due to the dimension of $\begin{bmatrix} {}^B\boldsymbol{R}_W\boldsymbol{F}; \boldsymbol{M} \end{bmatrix}$ is six, while the input dimension is eight (four tilting angles and four propeller spinning velocities).

Two common approaches to deal with the above challenges are performing nonlinear least-squares optimization (Johansen and Fossen, 2013) and using a nonlinear model-predictive controller (Prach and Kayacan, 2018). However, a severe problem in the two approaches is that the computational burden imposed on the quadrotor hardware is heavy, so it takes too high costs to implement the control allocation in real time.

Here, we propose a linear solution that first allocates the forces and moments to the vertical and lateral forces generated by each rotor, and then computes the tilting angles and motor speeds directly.

The thrust produced by each propeller (as shown in Figure 6) can be decomposed along the vertical and lateral direction into $\boldsymbol{N}_v$ and $\boldsymbol{N}_l$ as follows

$$N_{l,i} = T_i s(\alpha_i) = k_f n_i^2 s(\alpha_i) \tag{30}$$

$$N_{v,i} = T_i c(\alpha_i) = k_f n_i^2 c(\alpha_i). \tag{31}$$

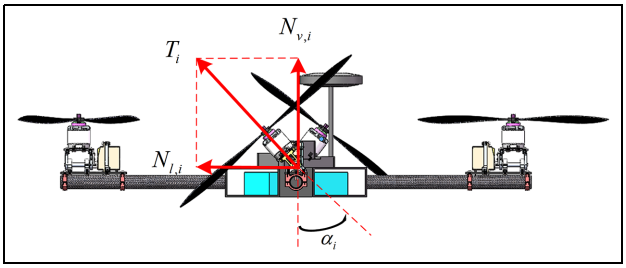

Figure 6. Descomposition of the propeller thrust.

The forces and moments $\begin{bmatrix} {}^B\boldsymbol{R}_W\boldsymbol{F}; \boldsymbol{M} \end{bmatrix}$ are linear combinations of $N_{l,i}$ and $N_{v,i}$. Therefore, equation (13) can be transformed to

$$\begin{bmatrix} {}^B\boldsymbol{R}_W\boldsymbol{F} \\ \boldsymbol{M} \end{bmatrix} = \boldsymbol{A}\,\boldsymbol{N}, \tag{32}$$

where $\boldsymbol{A}$ is a constant allocation matrix shown as (33) with dimensions of 6×8 and N is defined as the vector of all the vertical and lateral forces

$$\boldsymbol{A} = \begin{bmatrix} -\frac{\sqrt{2}}{2} & 0 & -\frac{\sqrt{2}}{2} & 0 & \frac{\sqrt{2}}{2} & 0 & \frac{\sqrt{2}}{2} & 0 \\ \frac{\sqrt{2}}{2} & 0 & -\frac{\sqrt{2}}{2} & 0 & -\frac{\sqrt{2}}{2} & 0 & \frac{\sqrt{2}}{2} & 0 \\ 0 & -1 & 0 & -1 & 0 & -1 & 0 & -1 \\ \frac{\sqrt{2}}{2}c_d & -\frac{\sqrt{2}}{2}l & -\frac{\sqrt{2}}{2}c_d & -\frac{\sqrt{2}}{2}l & -\frac{\sqrt{2}}{2}c_d & \frac{\sqrt{2}}{2}l & \frac{\sqrt{2}}{2}c_d & \frac{\sqrt{2}}{2}l \\ -\frac{\sqrt{2}}{2}c_d & \frac{\sqrt{2}}{2}l & -\frac{\sqrt{2}}{2}c_d & -\frac{\sqrt{2}}{2}l & \frac{\sqrt{2}}{2}c_d & -\frac{\sqrt{2}}{2}l & \frac{\sqrt{2}}{2}c_d & \frac{\sqrt{2}}{2}l \\ l & c_d & l & -c_d & l & c_d & l & -c_d \end{bmatrix}, \tag{33}$$

$$\boldsymbol{N} = [N_{l,1}, N_{v,1}, \ldots N_{l,4}, N_{v,4}]^{\mathrm{T}}, \tag{34}$$

Because $\boldsymbol{A}$ is independent of propeller tilting angles α, it is easy to calculate $\boldsymbol{N}$ from a desired $\begin{bmatrix} {}^B\boldsymbol{R}_W\boldsymbol{F}; \boldsymbol{M} \end{bmatrix}$ by inverting (32) as follows

$$\boldsymbol{N} = \boldsymbol{A}^+ \begin{bmatrix} {}^B\boldsymbol{R}_W\boldsymbol{F}_d \\ \boldsymbol{M}_d \end{bmatrix}. \tag{35}$$

Then, the actual tilting angle α_i and propeller thrust n_i can be obtained by

$$n_i = \frac{1}{k_f}\sqrt{N_{v,i}^2 + N_{l,i}^2}, \tag{36}$$

$$\alpha_i = \mathrm{a}\tan 2(N_{l,i}, N_{v,i}). \tag{37}$$

Closed-loop stability analysis

In this section, the closed-loop system is studied. First, the results on stability of the ESO is presented. Then, the stability of the inner control-loop (angular velocity control and velocity control) is studied. Finally, it is shown that if the inner control-loop is stable, the error of the outer control-loop can be confined in a finite (small) region.

Inner control-loop stability

As the angular velocity control and the velocity control are in the same control scheme, the following analysis is sufficient for both contro-loop. Define the observer error $\boldsymbol{e}_o$ for

$$\boldsymbol{e}_{o,\xi} = \boldsymbol{\xi} - \hat{\boldsymbol{\xi}}, \boldsymbol{e}_o, \boldsymbol{\zeta} = \boldsymbol{\zeta} - \hat{\boldsymbol{\zeta}}. \tag{38}$$

From (18), (19) and (26), (27), the common observer error dynamics can be written as

$$\dot{\boldsymbol{e}}_o = (\boldsymbol{A} - \boldsymbol{LC})\boldsymbol{e}_o + \boldsymbol{Eh}, \tag{39}$$

where $\boldsymbol{L} = [\beta_1 \boldsymbol{I} \quad \beta_2 \boldsymbol{I}]^T$, $\boldsymbol{C} = [\boldsymbol{I} \quad 0]$, $\boldsymbol{E} = [0 \quad \boldsymbol{I}]^T$ and

$$\boldsymbol{A} = \begin{bmatrix} 0 & \boldsymbol{I} \\ 0 & 0 \end{bmatrix}. \tag{40}$$

Theorem 1: Considering the observer error dynamics (39) under Assumption 1 and Assumption 2, if the observer gain vector $\boldsymbol{L}$ is chosen such that $(\boldsymbol{A} - \boldsymbol{LC})$ is stable, then the $\boldsymbol{e}_o$ exponentially converges to the bounded ball $\boldsymbol{B_{r1}} = \{\boldsymbol{e}_o \in \mathcal{R}^6 | \parallel \boldsymbol{e}_o \parallel \leqslant 2\boldsymbol{h}_{max}\lambda_{max}(\boldsymbol{P}_o)\}$, where $(\boldsymbol{A} - \boldsymbol{LC})^T\boldsymbol{P}_o + \boldsymbol{P}_o(\boldsymbol{A} - \boldsymbol{LC}) = -\boldsymbol{I}$, $\lambda_{max}(\boldsymbol{P}_o)$ is the maximum eigenvalue of $\boldsymbol{P}_o$ and $\boldsymbol{h}_{max}$ is the absolute maximum value of $\boldsymbol{h}$.

Proof: Define the Lyapunov function $\boldsymbol{V}_o$ as

$$\boldsymbol{V}_o = \boldsymbol{e}_o^T\boldsymbol{P}_o\boldsymbol{e}_o. \tag{41}$$

The derivative of $\boldsymbol{V}_o$ along the trajectories of (39) is given by

$$\begin{aligned} \dot{\boldsymbol{V}}_o &= \boldsymbol{e}_o^T[(\boldsymbol{A} - \boldsymbol{LC})^T\boldsymbol{P}_o + \boldsymbol{P}_o(\boldsymbol{A} - \boldsymbol{LC})]\boldsymbol{e}_o + 2\boldsymbol{e}_o^T\boldsymbol{P}_o\boldsymbol{Eh} \\ &\leqslant - \parallel \boldsymbol{e}_o\parallel^2 + 2\boldsymbol{h}_{max} \parallel \boldsymbol{P}_o \parallel\parallel \boldsymbol{e}_o \parallel \\ &\leqslant - \parallel \boldsymbol{e}_o \parallel (\parallel \boldsymbol{e}_o \parallel - 2\boldsymbol{h}_{max}\lambda_{max}(\boldsymbol{P}_o)). \end{aligned} \tag{42}$$

$\dot{\boldsymbol{V}}_o < 0$ whenever $\parallel \boldsymbol{e}_o \parallel > 2\boldsymbol{h}_{max}\lambda_{max}(\boldsymbol{P}_o)$.Thus, the $\boldsymbol{e}_o$ exponentially converges to the bounded ball $\boldsymbol{B}_{r1} = \{\boldsymbol{e}_o \in \mathcal{R}^6 | \parallel \boldsymbol{e}_o \parallel \leqslant 2\boldsymbol{h}_{max}\lambda_{max}(\boldsymbol{P}_o)\}$.

Next, consider the inner closed loop error dynamics. Define $\boldsymbol{e}_{cl}$ for

$$\boldsymbol{e}_{cl,\xi} = [\boldsymbol{\omega}_e \quad \boldsymbol{e}_{o,\xi}]^T, \boldsymbol{e}_{cl,\zeta} = [\boldsymbol{v}_e \quad \boldsymbol{e}_{o,\zeta}]^T, \tag{43}$$

the inner closed loop error dynamics can be written as

$$\dot{\boldsymbol{e}}_{cl} = \boldsymbol{A}_{cl}\boldsymbol{e}_{cl} + \boldsymbol{B}_1\boldsymbol{h} + \boldsymbol{B}_2\dot{\boldsymbol{d}}, \tag{44}$$

where $\boldsymbol{B}_1 = [0 \quad \boldsymbol{E}]^T$, $\boldsymbol{B}_2 = [(\boldsymbol{I} + \boldsymbol{K}_d)^{-1} \quad 0]^T$ and

$$\boldsymbol{A}_{cl} = = \begin{bmatrix} -(\boldsymbol{I} + \boldsymbol{K}_d)^{-1}\boldsymbol{K}_p & [0 \quad (\boldsymbol{I} + \boldsymbol{K}_d)^{-1}] \\ 0 & \boldsymbol{A} - \boldsymbol{LC} \end{bmatrix}. \tag{45}$$

For stability analysis results, the following assumption is made.

Assumption 3: The change rate of the desired angular velocity and the desired velocity of the inner loop, $\dot{\boldsymbol{\omega}}_d$ and $\dot{\boldsymbol{v}}_d$, are bounded.Thus, $\dot{\boldsymbol{d}}$ is bounded.

Theorem 2: Considering the closed loop error dynamics of (44) under Assumption 3, if the gain vector $\boldsymbol{K}_p$,$\boldsymbol{K}_d$ and the observer gain vector $\boldsymbol{L}$ are chosen such that $\boldsymbol{A}_{cl}$ is stable, then the $\boldsymbol{e}_{cl}$ exponentially converges to the bounded ball $\boldsymbol{B_{r2}} = \{\boldsymbol{e}_{cl} \in \mathcal{R}^6 | \parallel \boldsymbol{e}_{cl} \parallel \leqslant 2\boldsymbol{h}_{max}\lambda_{max}(\boldsymbol{P}_{cl}) + \frac{2}{1+k_d}\dot{\boldsymbol{r}}_{max}\lambda_{max}(\boldsymbol{P}_{cl})\}$, where $(\boldsymbol{A}_{cl})^T\boldsymbol{P}_{cl} + \boldsymbol{P}_{cl}(\boldsymbol{A}_{cl}) = -\boldsymbol{I}$, $\lambda_{max}(\boldsymbol{P}_{cl})$ is the maximum eigenvalue of $\boldsymbol{P}_{cl}$ and $\dot{\boldsymbol{d}}_{max}$ is the absolute maximum value of $\dot{\boldsymbol{d}}$.

Proof: Define the Lyapunov function $\boldsymbol{V}_{cl}$ as

$$\boldsymbol{V}_{cl} = \boldsymbol{e}_{cl}^T\boldsymbol{P}_{cl}\boldsymbol{e}_{cl}. \tag{46}$$

The derivative of $\boldsymbol{V}_{cl}$ along the trajectories of (44) is given by

$$\begin{aligned} \dot{\boldsymbol{V}}_{cl} &= \boldsymbol{e}_{cl}^T[(\boldsymbol{A}_{cl})^T\boldsymbol{P}_{cl} + \boldsymbol{P}_{cl}(\boldsymbol{A}_{cl})]\boldsymbol{e}_{cl} + 2\boldsymbol{e}_{cl}^T\boldsymbol{P}_{cl}\boldsymbol{B}_1\boldsymbol{h} + 2\boldsymbol{e}_{cl}^T\boldsymbol{P}_{cl}\boldsymbol{B}_2\dot{\boldsymbol{d}} \\ &\leqslant - \parallel \boldsymbol{e}_{cl}\parallel^2 + 2\boldsymbol{h}_{max} \parallel \boldsymbol{P}_{cl} \parallel\parallel \boldsymbol{e}_{cl} \parallel + 2\dot{\boldsymbol{d}}_{max} \parallel \boldsymbol{B}_2 \parallel\parallel \boldsymbol{P}_{cl} \parallel\parallel \boldsymbol{e}_{cl} \parallel \\ &\leqslant - \parallel \boldsymbol{e}_{cl} \parallel \left(\parallel \boldsymbol{e}_o \parallel - 2\boldsymbol{h}_{max}\lambda_{max}(\boldsymbol{P}_{cl}) - \frac{2}{1+k_d}\dot{\boldsymbol{d}}_{max}\lambda_{max}(\boldsymbol{P}_{cl})\right). \end{aligned} \tag{47}$$

$\dot{\boldsymbol{V}}_{cl} < 0$ whenever $\parallel \boldsymbol{e}_{cl} \parallel > 2\boldsymbol{h}_{max}\lambda_{max}(\boldsymbol{P}_{cl}) + \frac{2}{1+k_d}\dot{\boldsymbol{d}}_{max}\lambda_{max}(\boldsymbol{P}_{cl})$.Thus, the $\boldsymbol{e}_{cl}$ exponentially converges to the bounded ball $\boldsymbol{B_{r2}} = \{\boldsymbol{e}_{cl} \in \mathcal{R}^6 | \parallel \boldsymbol{e}_{cl} \parallel \leqslant 2\boldsymbol{h}_{max}\lambda_{max}(\boldsymbol{P}_{cl}) + \frac{2}{1+k_d}\dot{\boldsymbol{d}}_{max}\lambda_{max}(\boldsymbol{P}_{cl})\}$

Outer control-loop stability

The following theorem states that if the angular velocity control-loop is stable, then the attitude error is confined in a small region around $\boldsymbol{q}_e = \boldsymbol{q}_I$.

Assumption 4: The change rate of the desired attitude is zero. Thus, $\dot{\boldsymbol{q}}_d = 0$.

Theorem 3: Considering that Assumption 4 and the conditions of Theorem 2 hold, there exist constant, ε_ω, such that if $k_q > \varepsilon_\omega$, then the $\boldsymbol{q}_e$ is bounded to the region $\boldsymbol{Re_1} = \{\boldsymbol{q}_e | q_{0,e} \geqslant \sqrt{1 - (\frac{\varepsilon_\omega}{k_q})^2}, \parallel \boldsymbol{q}_{v,e} \parallel \leqslant \frac{\varepsilon_\omega}{k_q} \leqslant 1\}$, where ε_ω is the maximum of $\boldsymbol{\omega}_e$.

Proof: Differentiating from (22), the derivative of the attitude error is obtained as

$$\begin{aligned} \dot{\boldsymbol{q}}_e &= \boldsymbol{q}^{-1} \circ (\dot{\boldsymbol{q}}_d - \dot{\boldsymbol{q}} \circ \boldsymbol{q}_e) \\ &= -\boldsymbol{q}^{-1} \circ \dot{\boldsymbol{q}} \circ \boldsymbol{q}_e \\ &= -\frac{1}{2}[0 \quad \boldsymbol{\omega}]^T \circ \boldsymbol{q}_e \\ &= -\frac{1}{2}\begin{bmatrix} -\boldsymbol{q}_{v,e}^T\boldsymbol{\omega} \\ q_{0,e}\boldsymbol{\omega} + \boldsymbol{\omega} \times \boldsymbol{q}_{v,e} \end{bmatrix}. \end{aligned} \tag{48}$$

Define the Lyapunov function V_q as

$$V_q = q_{0,e}^2. \tag{49}$$

The derivative of V_q along trajectories of (51) is given by

Table 1. The gains of observers.

Gain	Value	Gain	Value
$\beta_{\xi,1}$	300	$\beta_{\xi,2}$	30000
$\beta_{\zeta,1}$	300	$\beta_{\zeta,2}$	30000

$$\begin{aligned}\dot{V}_q &= q_{0,e}\boldsymbol{q}_{v,e}^T\boldsymbol{\omega} \\ &= q_{0,e}\boldsymbol{q}_{v,e}^T(\boldsymbol{\omega}_d - \boldsymbol{\omega}_e) \\ &= q_{0,e}\boldsymbol{q}_{v,e}^T(-k_q sign(q_{0,e})\boldsymbol{q}_{v,e} - \boldsymbol{\omega}_e) \\ &\leqslant -|q_{0,e}| \parallel \boldsymbol{q}_{v,e} \parallel (k_q \parallel \boldsymbol{q}_{v,e} \parallel -\varepsilon_\omega) \\ &\leqslant -|q_{0,e}| \parallel \boldsymbol{q}_{v,e} \parallel (k_q\sqrt{1-q_{0,e}^2} - \varepsilon_\omega)\end{aligned} \tag{50}$$

Thus, if $k_q > \varepsilon_\omega$, $\dot{V}_q \leqslant 0$ whenever

$$-\sqrt{1-(\frac{\varepsilon_\omega}{k_q})^2} \leqslant q_{0,e} \leqslant \sqrt{1-(\frac{\varepsilon_\omega}{k_q})^2}, \tag{51}$$

which impiles that the attitude error $\boldsymbol{q}_e$ is bounded to the region $\boldsymbol{Re_1}$.

The following theorem states that if the velocity control-loop is stable, then the position error exponentially converges to a bounded ball.

Assumption 5: The change rate of the desired position is bounded. Thus, there exsits a constant $\beta_{\dot{p}_d}$ which is the maximum of the $\parallel \dot{\boldsymbol{p}}_d \parallel$.

Theorem 4: Considering that Assumption 5 and the conditions of Theorem 2 hold, there exist constant, ε_v, such that the $\boldsymbol{p}_e$ exponentially converges to the bounded ball $\boldsymbol{B_{r3}} = \{\boldsymbol{p}_e \in \mathcal{R}^3 | \parallel \boldsymbol{p}_e \parallel \leqslant \frac{\varepsilon_v + \beta_{\dot{p}_d}}{k}\}$, where ε_v is the maximum of $\parallel \boldsymbol{v}_e \parallel$.

Define the Lyapunov function V_p as

$$V_{\boldsymbol{p}} = \boldsymbol{p}_e^T\boldsymbol{p}_e. \tag{52}$$

The derivative of $V_{\mathbf{p}}$ is given by

$$\begin{aligned}\dot{V}_p &= 2\boldsymbol{p}_e^T\dot{\boldsymbol{p}}_e \\ &= 2\boldsymbol{p}_e^T(\dot{\boldsymbol{p}}_d - \dot{\boldsymbol{p}}) \\ &= -2\boldsymbol{p}_e^T\boldsymbol{v}_d + 2\boldsymbol{p}_e^T(\boldsymbol{v}_e + \dot{\boldsymbol{p}}_d) \\ &= -2\boldsymbol{p}_e^T\boldsymbol{K}\boldsymbol{p}_e + 2\boldsymbol{p}_e^T(\boldsymbol{v}_e + \dot{\boldsymbol{p}}_d) \\ &\leqslant -2k \parallel \boldsymbol{p}_e\parallel^2 + \parallel \boldsymbol{p}_e \parallel (\varepsilon_v + \beta_{\dot{p}_d}) \\ &\leqslant -2 \parallel \boldsymbol{p}_e \parallel (k \parallel \boldsymbol{p}_e \parallel -\varepsilon_v - \beta_{\dot{p}_d})\end{aligned} \tag{53}$$

Thus, $\dot{V}_p \leqslant 0$ whenever $\parallel \boldsymbol{p}_e \parallel \geqslant \frac{\varepsilon_v + \beta_{\dot{p}_d}}{k}$, which means that the position error $\boldsymbol{p}_e$ exponentially converges to the bounded ball $\boldsymbol{B_{r3}}$.

Simulation results

In this section, we show the results obtained in a series of simulations to verify the effectiveness and robustness of the proposed control scheme. The specific parameters of the quadrotor with tiltable rotors are: $m = 2.274$ kg, $\boldsymbol{J}_B = \text{diag}[0.021231 \quad 0.021231 \quad 0.042117]\,\text{kgm}^2$, $l = 0.325m$, $k_f = 3.098E-5$,$c_d = 0.181$. The gains of the ESO are tuned according to Gao (2003) (Table 1).

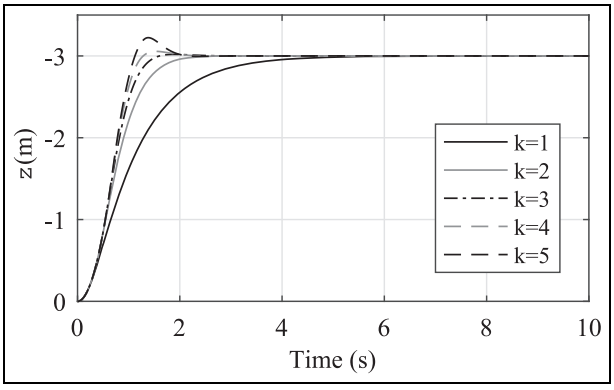

Figure 7. The effects of k changes.

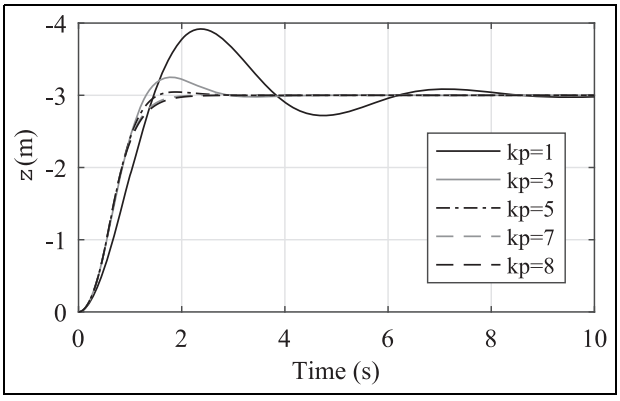

Figure 8. The effects of k_p changes.

Controller gains tuning

The selection of parameters directly affects the control performances. The controller gains need to be tuned, including $\boldsymbol{K}/k_q$ in the outer control-loop and $\boldsymbol{K}_p, \boldsymbol{K}_d$ in the inner control-loop. Taking the step response of z chanel ($z_d = -3$) as an example, guidances of controller gains tuning are presented in the following.

The gain k directly affect the ascent speed. As shown in Figure 7, higher gain k results in faster ascent speed. However, if the gain k is too high, then the overshoot becomes bigger as well.

The responses of k_p and k_d change are reported in Figure 8 and Figure 9 and the gain k_p influences the overshoot and oscillation. Increasing the gain k_p can decrease the overshoot and the number of oscillations. The overshoot is also affected by the gain k_d. While increasing the gain k_d leads to smaller overshoot, it also delays the rise of the output.

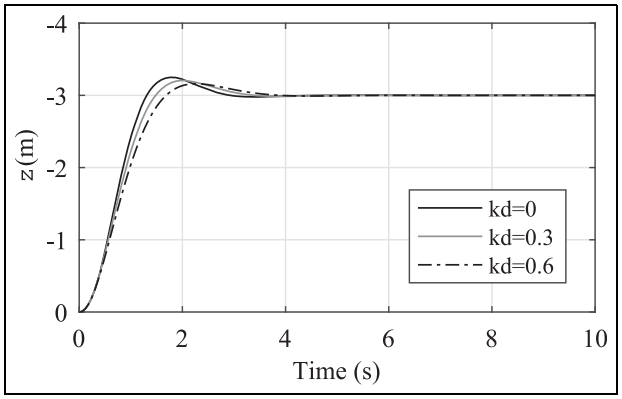

Figure 9. The effects of k_d changes.

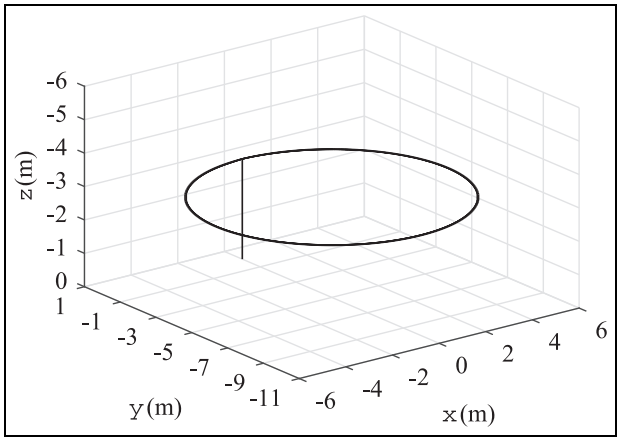

Figure 10. Case a: Position outputs.

Table 2. The gains of controllers and observers.

Gain	Value	Gain	Value
k_x	2	k_y	2
k_z	2	k_q	3.8
$k_{v_x,p}$	8	$k_{v_y,p}$	8
$k_{v_z,p}$	8	$k_{v_x,d}$	0.8
$k_{v_y,d}$	0.8	$k_{v_z,d}$	0.8
$k_{\omega_x,p}$	8	$k_{\omega_y,p}$	8
$k_{\omega_z,p}$	8	$k_{\omega_x,d}$	0.8
$k_{\omega_y,d}$	0.8	$k_{\omega_z,d}$	0.8

Overall, the controller gains tuning process of proposed method is similar to the cascade PD control as long as the observer gains are well-tuned. The controller gains used in the following simulation are shown in Table 2.

Case a: Flight with zero-level attitude

In the first simulation, the desired position reference involves a circular trajectory

$$\boldsymbol{p}_d = \begin{bmatrix} 5\sin(\frac{\pi}{10}(t-5)) \\ 5\cos(\frac{\pi}{10}(t-5)) - 5 \\ -3 \end{bmatrix} \tag{54}$$

while the desired attitude is given by $\boldsymbol{q}_d = \boldsymbol{q}_I$. The considered omnidirectional maneuver is not feasible for the popular multirotor platform. The reference position trajectory (dotted line) and the actual path (solid line) of the vehicle are shown in Figure 10.

The vehicle is required to keep a zero-level attitude and hold the heading direction still: the attitude error in terms of roll-pitch-yaw angle errors are reported in Figure 11. The results show that the proposed control method has excellent performance of position tracking while holding the orientation (the maximum angle error is no more than 1 degree).

Case b: Rotation on the spot

The second simulation shows the performance of the proposed controller of attitude tracking while keeping the vehicle position on the spot. Figure 12 shows the evolution of the vehicle's desired attitude and the actual attitude. Even though the desired attitude is changed every moment, the proposed controller can drive the attitude to the new reference attitude despite being affected by the Coriolis term. The following two simulations will further test the robustness of the proposed controller under external disturbances and parameter uncertainties. Figure 13 shows the horizontal position errors and evolution of the vertical position. The vehicle can maintain its position when rotating.

Case c: Hovering with constant attitude under disturbances

To verify the performance of the proposed controller under external disturbances, the following aerodynamics forces and moments are considered (which refers to Mokhtari et al., 2016)

$$\frac{1}{m}\boldsymbol{F}_\delta = \begin{bmatrix} \sin(t) + 2 \\ \cos(t) + 2 \\ \sin(t) + 2 \end{bmatrix}, \tag{55}$$

$$\boldsymbol{M}_\delta = \begin{bmatrix} 0.3\sin(0.5t) + 0.6 \\ 0.3\cos(0.5t) + 0.6 \\ 0.3\sin(t) + 0.6 \end{bmatrix}. \tag{56}$$

The initial states of the vehicle are set as $\boldsymbol{p} = [0 \quad 0 \quad 0]$, $\phi = 0, \theta = 0, \psi = 0$. It is required to reach states: $\boldsymbol{p}_d = [0 \quad 0 \quad -3]$, $\phi_d = 10, \theta_d = 15, \psi_d = 20$ and then hold.

Figure 14 shows the comparison between the absolute position outputs obtained using PID (dotted line) and the proposed method (solid line) in the presence of the superior force and moment disturbances. Also, the comparison of attitude outputs is reported in Figure 15. From these figures, it can been seen that both the position and attitude of the vehicle controlled by PID can not converge to the references but fluctuate over the targets. However, the proposed controller can drive the position and attitude to the references quickly and robustly in spite of the disturbances, as the ESO can estimate and compensate the forces and moments accurately (the comparison between the real disturbance $M_{\delta,x}$ and the

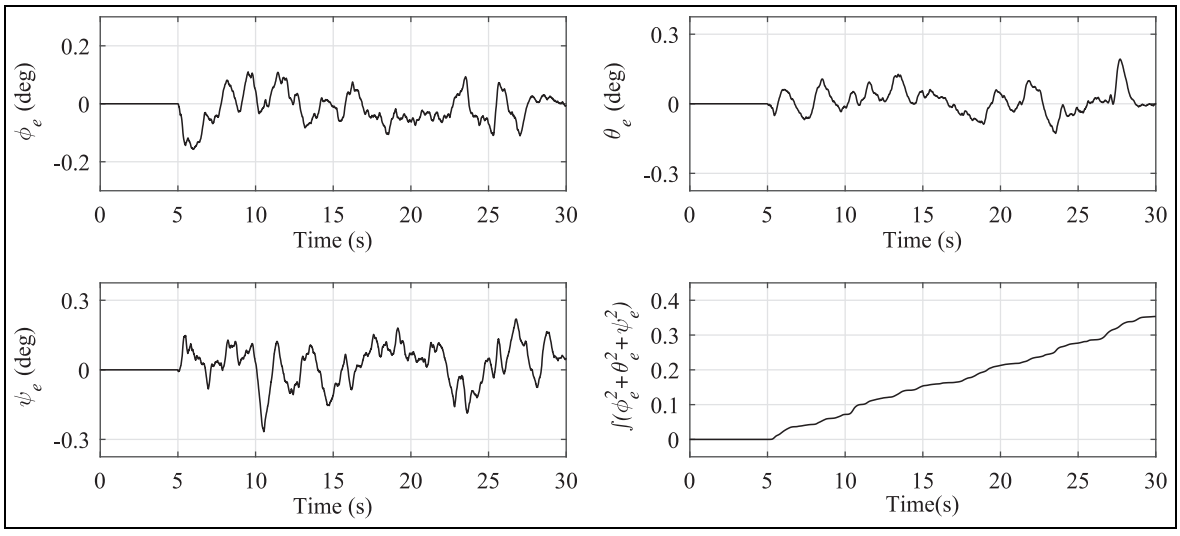

Figure 11. Case a: Attitude error in terms of roll-pitch-yaw angle errors.

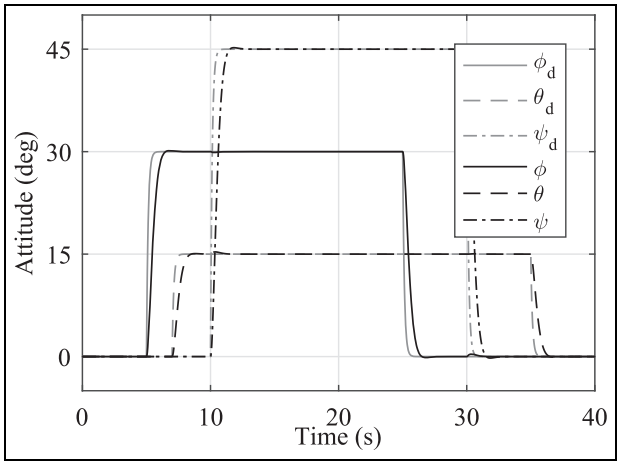

Figure 12. Case b: Attitude outpus in terms of roll-pitch-yaw angle.

estimation $\dot{M}_{\delta,x}$ is shown in Figure 16). Besides, it can be seen that the control input is big in the beginning because the error is large from Figure 17 and Figure 18. This feature is similar to the PD control, which means the proposed method does not impove the perfomance in this aspect. More improvements of control input should be sought in the future development.

Case d: System parameters change

To verify the control performance under the parameter uncertainties, simulations of increasing and decreasing the quadrotor inertia by 50% are carried out. The desired roll angle ϕ_d is set to 10 (deg) and the controller and observer gains are hold still. Figure 19 showns the step response of roll angle. Although the parameter changes, the step response changes a little, which means that the proposed controller is robust to the parameter uncertainties.

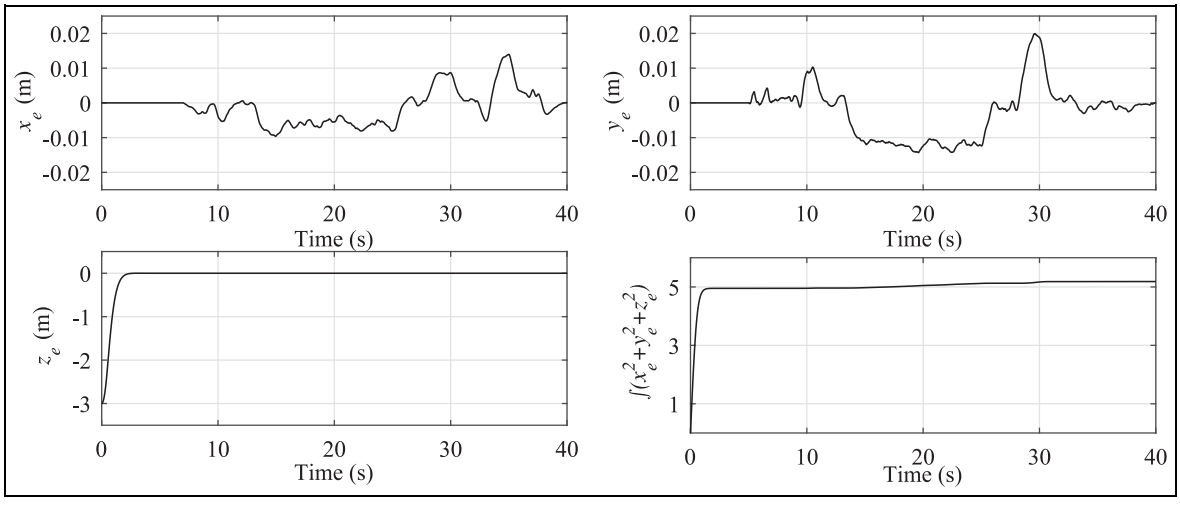

Figure 13. Case b: Horizontal position error and vertical position evolution.

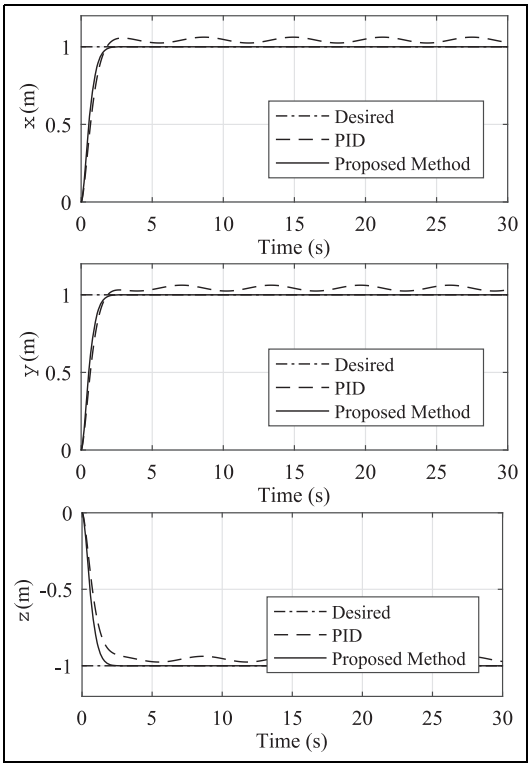

Figure 14. Case c: Position outputs.

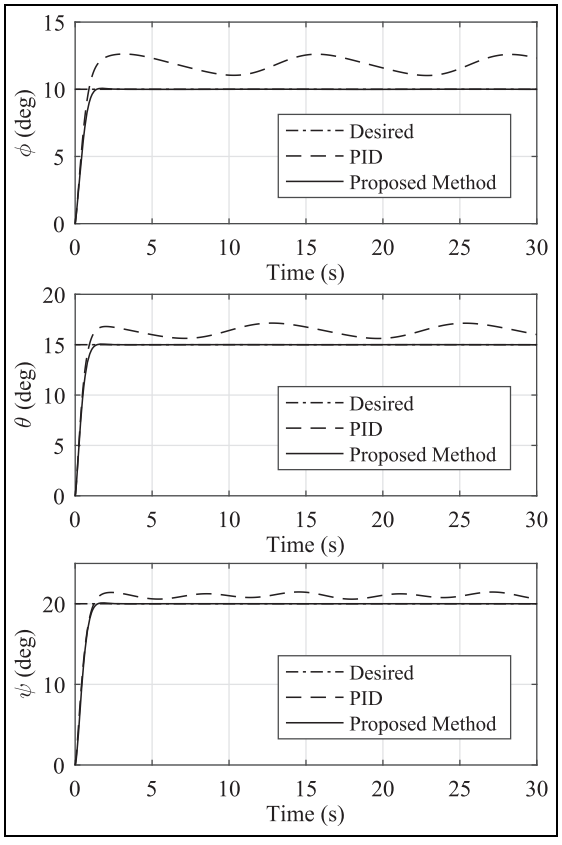

Figure 15. Case c: Attitude outputs.

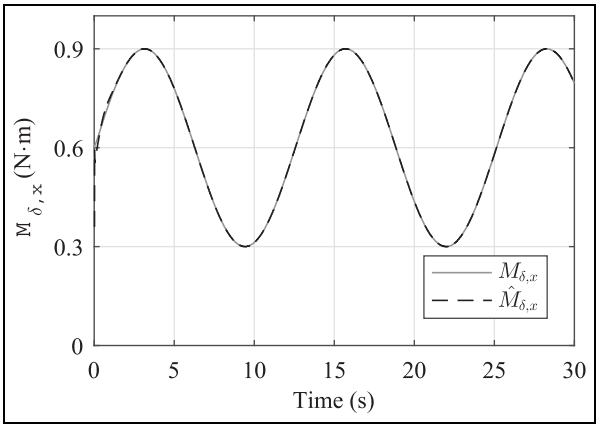

Figure 16. Case c: Estimation of the total disturbances.

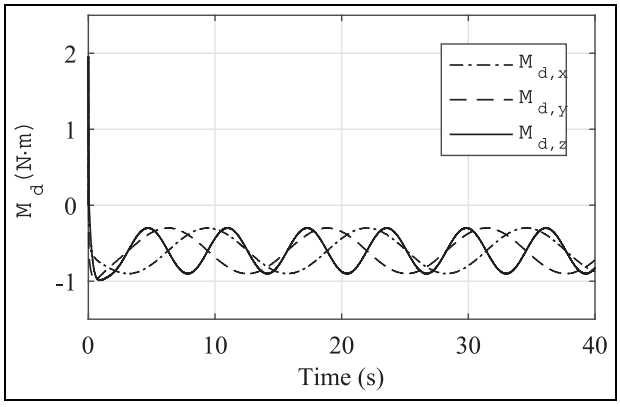

Figure 17. Case c: Control input of attitude controller.

Conclusion

This paper presented a solution to the problem of omnidirectional control of a quadrotor with tiltable rotors. The conventional hypothesis of knowledge of inertia parameters and absence of external disturbances are avoided in the controller design. Indeed, we propose a control strategy based on the ESO integrated with PD controller to solve the omnidirectional control of autonomous quadrotors with tiltable rotors in the presence of model parameter uncertainties and unknown external efforts. Thanks to the dynamical structure model of the omnidirectional quadrotor, a particular parallel flight control approach is applied. The proposed control technique combines the advantage of the ESO to estimate and compensate the total external disturbances and that of the PD controller to drive the state of the omnidirectional copter closed-loop system to converge to the references. Moreover, in the control allocation design, the nonlinear control allocation matrix is linearized by variable substitution. Simulations demonstrate that the proposed controller has good performances and fine stability of omnidirectional maneuver control.

As future work, it would be anticipated to design a new mechanism for the omnidirectional quadrotor in the

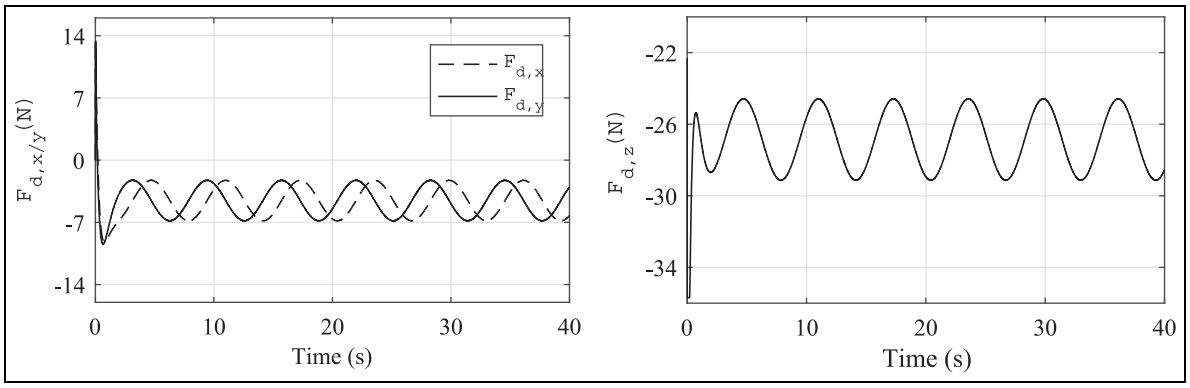

Figure 18. Case c: Control input of position controller.

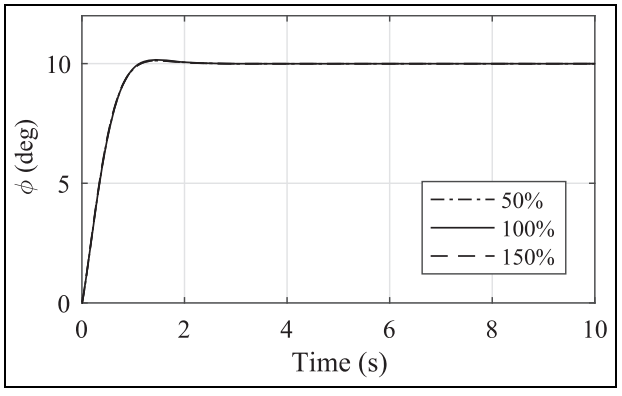

Figure 19. The effects of system parameter changes.

physically interactive tasks. Also, it would be interesting to improve the control performances by considering the interaction forces.

Declaration of conflicting interests

The author(s) declared no potential conflicts of interest with respect to the research, authorship, and/or publication of this article.

Funding

The author(s) disclosed receipt of the following financial support for the research, authorship, and/or publication of this article: This paper was support by National Natural Science Foundation of China (Grant No. 6147314), the Science and Technology Projects of China Southern Power Grid (Grant No. 066600KK52170074), the Foundation of Graduate Innovation Center in NUAA (Grant No. kfjj20190301).

ORCID iDs

Kaiwen Lu https://orcid.org/0000-0003-2618-3733
Zhong Yang https://orcid.org/0000-0002-0988-3757

References

Barikbin B and Fakharian A (2019) Trajectory tracking for quadrotor UAV transporting cable-suspended payload in wind presence. *Transactions of the Institute of Measurement and Control* 41(5): 1243–1255.

Benallegue A, Mokhtari A and Fridman L (2008) Highorder slidingmode observer for a quadrotor UAV. *International Journal of Robust and Nonlinear Control: IFAC-Affiliated Journal* 18(4-5): 427–440.

Castillo A, Sanz R, Garcia P, et al. (2019) Disturbance observer-based quadrotor attitude tracking control for aggressive maneuvers. *Control Engineering Practice* 82(2019): 14–23.

Chovancov A, Fico T, Chovanec L, et al. (2014) Mathematical modelling and parameter identification of quadrotor (a survey). *Procedia Engineering* 96(2014): 172–181.

Crowther B, Lanzon A, Maya-Gonzalez M, et al. (2011) Kinematic analysis and control design for a nonplanar multirotor vehicle. *Journal of Guidence, Control, and Dynamics* 34(4): 1157–1171.

Dyer E, Sirouspour S and Jafarinasab M (2019) Energy optimal control allocation in a redundantly actuated omnidirectional UAV. In: 2019 *IEEE International Conference on Robotics and Automation (ICRA)*, Montreal, QC, 20–24 May 2019, pp. 5316–5322. New York: IEEE.

Gao Z (2003) Scaling and bandwidth-parameterization based controller tuning. In: *2006 American Control Conference*, Denver, CO, 4–6 June 2003, pp. 4989–4996. New York: IEEE.

Gassner M, Cieslewski T and Scaramuzza D (2017) Dynamic collaboration without communication: Vision-based cable-suspended load transport with two quadrotors. In: *2017 IEEE International Conference on Robotics and Automation (ICRA)*, Singapore, 29 May–3 June 2017, pp. 5196–5202. New York: IEEE.

Han J (2009) From PID to active disturbance rejection control. *IEEE Transactions on Industrial Electronics* 56(3): 900–906.

He M and He J (2018) Extended state observer-based robust backstepping sliding mode control for a small-size helicopter. *IEEE Access* 6(2018): 33480–33488.

Johansen TA and Fossen TI (2013) Control allocation: A survey. *Automatica* 49(5): 1087–1103.

Kamel M, Verling S, Elkhatib O, et al. (2018) The voliro omniorientational hexacopter: An agile and maneuverable tiltable-rotor aerial vehicle. *IEEE Robotics and Automation Magazine* 25(4): 34–44.

Kaufman E, Caldwell K, Lee D, et al. (2014) Design and development of a free-floating hexrotor UAV for 6-DOF maneuvers. In: *2014 IEEE Aerospace Conference*, Big Sky, MT, 1–8 March 2014, pp. 1–10. New York: IEEE.

Korpela C, Orsag M and Oh P (2014) Towards valve turning using a dual-arm aerial manipulator. In: *2014 IEEE/RSJ International Conference on Intelligent Robots and Systems (IROS)*, Chicago, IL, 14–18 September 2014, pp. 3411–3416. New York: IEEE.

Lazim IM, Husain AR, Mohamed Z, et al. (2019) Disturbance observer-based formation tracking control of multiple quadrotors in the presence of disturbances. *Transactions of the Institute of Measurement and Control* 41(14): 4129–4141.

Liu H, Zhao W, Zuo Z, et al. (2017) Robust control for quadrotors with multiple time-varying uncertainties and delays. *IEEE Transactions on Industrial Electronics* 64(2): 1303–1312.

Liu J, Vazquez S, Wu L, et al. (2017) Extended state observer-based sliding-mode control for three-phase power converters. *IEEE Transactions on Industrial Electronics* 64(1): 22–31.

Mokhtari MR, Braham AC and Cherki B (2016) Extended state observer based control for coaxial-rotor UAV. *ISA Transactions* 61(2016): 1–14.

Oosedo A, Abiko S, Narasaki S, et al. (2015) Flight control systems of a quad tilt rotor unmanned aerial vehicle for a large attitude change. In: *2015 IEEE International Conference on Robotics and Automation*, Seattle, WA, 26–30 May 2015, pp. 2326–2331. New York: IEEE.

Park S, Her J, Kim J, et al. (2016) Design, modeling and control of omni-directional aerial robot. In: *2016 IEEE/RSJ International Conference on Intelligent Robots and Systems (IROS)*, Daejeon, 9–14 October 2016, pp. 1570–1575. New York: IEEE.

Park S, Lee J, Ahn J, et al. (2018) ODAR: Aerial manipulation platform enabling omnidirectional wrench generation. *IEEE/ASME Transactions on Mechatronics* 23(4): 1907–1918.

Pounds PE, Mahony R and Corke P (2010) Modelling and control of a large quadrotor robot. *Control Engineering Practice* 18(7): 691–699.

Prach A and Kayacan E (2018) An MPC-based position controller for a tilt-rotor tricopter VTOL UAV. *Optimal Control Applications and Methods* 39(1): 343–356.

Rajappa S, Ryll M, Blthoff HH, et al. (2015) Modeling, control and design optimization for a fully-actuated hexarotor aerial vehicle with tilted propellers. In: *2015 IEEE International Conference on Robotics and Automation (ICRA)*. Seattle, WA, 26–30 May 2015, pp. 4006–4013. New York: IEEE.

Rashad R, Califano F and Stramigioli S (2019) Port-Hamiltonian passivity-based control on SE(3) of a fully actuated UAV for aerial physical interaction near-hovering. *IEEE Robotics and Automation Letters* 4(4): 4378–4385.

Ryll M, Blthoff HH and Giordano PR (2012) Modeling and control of a quadrotor UAV with tilting propellers. In: *2012 IEEE International Conference on Robotics and Automation (ICRA)*, Saint Paul, MN, 14–18 May 2012, pp. 4606–4613. New York: IEEE.

Ryll M, Blthoff HH and Giordano PR (2013) First flight tests for a quadrotor UAV with tilting propellers. In: *2013 IEEE International Conference on Robotics and Automation*, Karlsruhe, 6–10 May 2013, pp. 295–302. New York: IEEE.

Ryll M, Blthoff HH and Giordano P R (2015) A novel overactuated quadrotor unmanned aerial vehicle: modeling, control, and experimental validation. *IEEE Transactions on Control Systems Technology* 23(2): 540–556.

Ryll M, Bicego D and Franchi A (2016) Modeling and control of FAST-Hex: A fullyactuated by synchronized-tilting hexarotor. In: *2016 IEEE/RSJ International Conference on Intelligent Robots and Systems (IROS)*, Daejeon, 9–14 October 2016, pp. 1689–1694. New York: IEEE.

Shi D, Wu Z and Chou W (2019) Anti-disturbance trajectory tracking of quadrotor vehicles via generalized extended state observer. *Journal of Vibration and Control* 26(13–14): 1173–1186.

Shuster MD (1993) A survey of attitude representations. *Journal of the Astronautical Sciences* 41(4): 439–517.

Thomas J, Loianno G, Sreenath K, et al. (2014) Toward image based visual servoing for aerial grasping and perching. In: *2014 IEEE International Conference on Robotics and Automation (ICRA)*. Hong Kong, 31 May–7 June 2014, pp. 21132118. New York: IEEE.

Wang W and Gao Z (2003) A comparison study of advanced state observer design techniques. In: *2003 American Control Conference*, Denver, CO, 4–6 June 2003, pp. 47544759. New York: IEEE.

Yao J, Jiao Z and Ma D (2014) Extended-state-observer-based output feedback nonlinear robust control of hydraulic systems with backstepping. *IEEE Transactions on Industrial Electronics* 61(11): 6285–6293.